Optical Properties of Some $Pb_{1-x}Sn_xTe$ Alloys Determined from Infrared Plasma Reflectivity Measurements*

Gaston Dionne
Hydro-Québec Institute of Research, Varennes, Québec, Canada
and
John C. Woolley
University of Ottawa, Ottawa, Ontario, Canada
(Received 25 April 1972)

The infrared reflectivity was measured as a function of hole concentration at 82 °K for $Pb_{1-x}Sn_xTe$ alloy samples with $x = 0.06$ and 0.21 and as a function of temperature for one sample with $x = 0.21$ and hole concentration 8.7×10^{18} cm^{-3}. The measured reflectivity spectra were remarkably well fitted by the classical free-carrier dispersion relations. The optical dielectric constant ϵ_∞, the susceptibility effective mass m_s, and the optical mobility μ_{opt} were determined from a curve-fitting technique and a minimum-reflectivity technique generalized to include the effect of nondegeneracy. Using the former technique, a second valence-band maximum situated at about 0.23 eV below the main valence-band maximum was detected in the alloy with $x = 0.21$. The energy gap and ϵ_∞ were found to be related by $\ln E_G = 0.086\epsilon_\infty + 1.65$ in lead-rich $Pb_{1-x}Sn_xTe$ alloys. The optical mobility was found to be about a factor of 2 lower than the conductivity mobility in all samples measured. The experimental values of m_s were compared with those expected from the Kane, Cohen, and Dimmock models. The results of these comparisons indicate that the two-band models of Kane and Cohen, especially the former, are more suitable than the six-band model of Dimmock to explain the carrier-concentration dependence of m_s, and that none of the models account for the large increase of m_s with temperature.

I. INTRODUCTION

The L symmetry of the main valence- and conduction-band extrema appears to be well established in PbTe and in lead-rich $Pb_{1-x}Sn_xTe$ alloys. Because of the small energy gap, both conduction and valence bands are nonparabolic and their nonparabolicity is due mainly to the interaction of these two bands.[1] In fact, the two-band models, such as the Cohen and the Kane models, have been used with some success to explain experimental data in PbTe.[2-4] However, theoretical band investigations[5,6] show that there are six relatively closely spaced $\langle 111 \rangle$ bands near the Fermi level, the interactions of which need to be considered to determine the nonparabolicity of the valence and conduction bands. Also, in p-type $Pb_{1-x}Sn_xTe$, while most of the carriers are in the $\langle 111 \rangle$ extrema, there is evidence for extra band maxima contributing to conduction.[3,7,8] This further complicates the situation in p-type material because the nonparabolicity effects and the heavy-mass band effects are often difficult to distinguish.

One of the best tools to investigate the nonparabolicity and the presence of extra bands participating in conduction is the determination of susceptibility effective masses from measurements of infrared reflectivity. These measurements can be made over a large range of carrier concentration and temperature. To quote Dixon and Riedl[2] "they serve as a stringent consistency test of proposed band models and their parameters." In the present experiment, we chose to investigate p-type $Pb_{1-x}Sn_xTe$ alloys with $x = 0.06$ and 0.208 because their band structures at $\langle 111 \rangle$ resemble that of PbTe. Also, it was expected, since the main gap varies appreciably with alloying, that the relative position of all the band extrema participating in conduction would change sufficiently to give new manifestations of their presence.

In order to extract more information from the experiments, the reflectivity measurements were analyzed in terms of classical dispersion models using both the fitting technique first used by Dixon and Riedl[2] and the Moss *et al.* technique.[9] The susceptibility effective-mass results have been presented so as to illustrate the advantages of using the two methods of analysis in the present case. Also, additional data concerning the high-frequency dielectric constant and the optical mobility have been given. Finally, the predictions of the two-band Kane and Cohen models and of the six-band Dimmock model have been compared with the experimental results.

II. EXPERIMENTAL

The reflectivity measurements were made using a Baird Associate spectrometer equipped with either an NaCl or a KBr prism for the shorter (4–15-μ) and the longer (12–22-μ) wavelengths,

respectively. The light from the exit slit of the spectrometer was collected using a large spherical mirror which focused a small image of the exit slit on the sample. The light reflected from the sample was in turn focused onto the detector using a short focal-length ellipsoidal mirror which was adjusted so that the final image of the exit slit was centered and within the sensitive area of the bolometer detector. The samples and the aluminum mirror were mounted on the cold finger of an optical Dewar similar to that described by Fortin.[10] Rotation about the axis of the cold finger was possible for both the samples and the windows independently. This allowed for sample and the window to be adjusted so that only the light reflected from the sample was collected, the light reflected from the window being eliminated in a systematic way. The temperatures were measured to within 1 °K using a copper-constantan thermocouple soldered to the copper cold finger. The angle of incidence of the light on the sample was about 10° and 15° from normal for the central and extreme rays, respectively. For these angles of incidence the reflectivity was the same as that obtained at normal incidence to within 1%. The reflectivity was determined by taking the ratio of the intensity reflected from the sample to that reflected from a front-surface aluminum mirror.

The samples were single-crystal $Pb_{1-x}Sn_xTe$ alloys grown in our laboratory using the Bridgman technique. For each of the two single-crystal ingots used, several samples were cut from one circular disk (14 mm in diameter and 3 mm thick) taken from the first quarter of the ingot to freeze. In this way, the composition gradients across the samples were kept smaller than about $x = 0.003$ in all cases. The compositions of the two sets of rectangular parallelepipeds (approximately $9 \times 2 \times 1$ mm) were $x = 0.060$ and 0.208, respectively. The various carrier concentrations were obtained by heat treatment following which about 100 μ of material was removed from all six faces of the samples to eliminate the carrier-concentration gradient often present in a thin surface layer after the heat treatment. The growth, characterization, and heat treatment are described in detail elsewhere.[11]

The samples were prepared for the reflectivity measurements by removing the damaged surface layers through the following steps: (i) a deep (~ 50 μ) chemical etching using a procedure and an etch similar to that described by Coates *et al*[12]; (ii) a light mechanical polishing with 0.1–0.01-μ powder to restore the flatness of the surface; (iii) and finally, shallow (~ 10 μ) chemical etching that left the surface flat and mirrorlike in appearance. Using the above procedure, Laue photographs, taken with low (10-kV) x-ray-tube voltage to minimize the x-ray penetration depth, indicated that the surfaces were free of major damage and strains. Also, the measured reflectivity spectra were reproducible and well fitted (see Fig. 5) by those calculated from Eqs. (1), (4), and (5) given below. This indicates that these reflectivities are characteristic of the bulk rather than a damaged surface layer. As has been found previously[2,13,14] when the surface preparation was terminated with mechanical polishing these conditions were not realized. Thus, in the present work, only the reflectivity spectra obtained from surfaces prepared according to the full procedure described above were analyzed.

The values of the carrier concentration N and of the conductivity mobility μ_c were determined from measurements of the weak-field Hall coefficient R_0 and of the conductivity σ using the relations $N = (r/R_0 e)_{77°K}$ and $\mu_c = \sigma/Ne$. In these equations $r = R_0/R_\infty$, where R_∞ is the high-field Hall coefficient. With available magnetic fields, r could be measured in the lowest carrier-concentration samples only. Its value was close to 0.9 for both alloy compositions studied. In the absence of any direct experimental determination of r at higher carrier concentration in the alloys studied, we have defined a quantity $p^* = (0.9/R_0 e)_{77°K}$, which has been used in the analysis of the reflectivity measurements. However, in Sec. V, the final results were corrected using semiempirical values of r versus carrier concentration. We postpone this discussion to Sec. V. Table I lists the samples and their electrical properties. The last three columns make use of the values of r versus carrier concentration given in Fig. 7(b).

III. THEORY

A. Classical Dispersion Equations

The reflectivity R at normal incidence on thick specimens in air or vacuum is given in terms of the index of refraction η and the extinction coefficient κ by

$$R = \frac{(\eta - 1)^2 + \kappa^2}{(\eta + 1)^2 + \kappa^2} \quad . \tag{1}$$

It is related to the complex dielectric constant $\tilde{\epsilon}$ through the defining equations:

$$\tilde{\epsilon} \equiv \epsilon_1 + i\epsilon_2 = \eta^2 - \kappa^2 + 2i\eta\kappa \quad . \tag{2}$$

The knowledge of the pairs (η, κ) or (ϵ_1, ϵ_2) fully describes the phenomenon of reflection macroscopically through Maxwell's equations. These pairs are usually related to models which describe the physical processes on the atomic scale, using the simplifying assumption that the effective field is the same as the externally applied field.[15–17] A consequence of this assumption is that the dif-

TABLE I. Electrical properties of p-type $Pb_{1-x}Sn_xTe$ samples at 77.3 °K.

Sample No.	$p^* = (0.9/R_0e)_{77\,°K}$ (cm^{-3})	μ_c (77 °K) (cm^2/V sec)	R_0/R_∞ (77 °K)[a]	N (77 °K) (cm^{-3})
		20.8-mol% SnTe		
8-3	1.192×10^{20}	205	0.80	1.05×10^{20}
8-5	1.055×10^{20}	258	0.73	8.5×10^{19}
8-6	9.864×10^{19}	351	0.60	6.6×10^{19}
8-1	4.586×10^{19}	874	0.70	3.57×10^{19}
8-2	1.926×10^{19}	2184	0.76	1.63×10^{19}
8-7	9.765×10^{18}	4087	0.80	8.68×10^{18}
8-4	6.406×10^{18}	5740	0.82	5.84×10^{18}
8-8	2.56×10^{18}	10400	0.86	2.45×10^{18}
		6-mol% SnTe		
6-1	2.882×10^{19}	1150	0.73	2.34×10^{19}
6-0	1.116×10^{19}	3240	0.79	9.8×10^{18}
6-6	5.805×10^{18}	5670	0.82	5.3×10^{18}
6-3	4.66×10^{17}	15900	0.90	4.66×10^{17}

[a]From Fig. 7(b) (see text).

ferent contributions to the dielectric constant in cubic material are additive:

$$\tilde{\epsilon} = 1 + \tilde{\epsilon}_{BC} + \tilde{\epsilon}_{FC} + \tilde{\epsilon}_{LV} , \tag{3}$$

in which the $\tilde{\epsilon}$'s represent the contributions of bound carriers, free carriers, and lattice vibration, respectively. For wavelengths somewhat beyond the fundamental absorption edge and shorter than that of the longitudinal optical mode λ_L, the imaginary part of $\tilde{\epsilon}_{BC}$ and $\tilde{\epsilon}_{LV}$ may be neglected,[16,17] and their real parts written as

$$\epsilon_{BC} = \epsilon_\infty + \Delta\epsilon_\infty(\lambda)$$

and[2,16]

$$\epsilon_{LV} = -(1 - \epsilon_\infty/\epsilon_S)(\epsilon_\infty/\lambda_L^2)\lambda^2 ,$$

respectively. In these expressions, the optical dielectric constant ϵ_∞ is the bound-carrier contribution at wavelengths well beyond the fundamental absorption edge, $\Delta\epsilon_\infty(\lambda)$ is its wavelength-dependent deviation from ϵ_∞ near the fundamental absorption edge, and ϵ_S is the static dielectric constant. The complete equations, including the free-carrier dispersion and absorption[17] and taking into account the distributions of scattering times τ and effective masses m through approximations, [18–20] are (in mks units)

$$\eta^2 - \kappa^2 - \epsilon_t = \frac{-Ne^2}{m_s\epsilon_0} \frac{a^2\langle\tau\rangle^2}{1+\omega^2a^2\langle\tau\rangle^2} , \tag{4}$$

$$2\eta\kappa = \frac{Ne^2}{m_s\epsilon_0\omega} \frac{\langle\tau\rangle}{1+\omega^2a^2\langle\tau\rangle^2} , \tag{5}$$

in which

$$\epsilon_t = \epsilon_\infty + \Delta\epsilon_\infty(\lambda) - (1 - \epsilon_\infty/\epsilon_S)(\epsilon_\infty/\lambda_L^2)\lambda^2 ,$$

where λ and ω are the wavelength and the angular frequency of the infrared radiation, ϵ_0 is the permittivity of free space, N is the carrier concentration, m_s is the susceptibility effective mass given by $1/m_s \equiv \langle 1/m\rangle$, and $a^2 = \langle\tau^2\rangle/\langle\tau\rangle^2$, in which the bracket signifies average over the distribution. We also define the optical mobility as $\mu_{opt} \equiv e\langle\tau\rangle/m_s$.

The validity of the approximations involved in the average over the distribution of scattering times in Eqs. (4) and (5) has been discussed elsewhere.[9,18–21] In the present experiment, it introduces negligible error in the determination of the susceptibility effective mass m_s because $\omega\tau > 3$ (see Tables III and IV) and the statistics are sufficiently degenerate [see Fermi energies in Figs. 13(c) and 15(a)]. For nonparabolic bands, there is a distribution of effective masses m as well as of scattering times τ. Thus, to bring out explicitly the ω, τ, and m_s dependence in Eq. (4), it is necessary to make the additional approximation

$$\left\langle \frac{1}{m} \frac{\tau^2}{1+\omega^2\tau^2} \right\rangle \simeq \left\langle \frac{1}{m} \right\rangle \left\langle \frac{\tau^2}{1+\omega^2\tau^2} \right\rangle .$$

This later approximation introduces negligible error in the determination of m_s in the present case. This is because for sufficiently large $\omega\tau$ values the bracketed term containing τ does not vary much with carrier energy since τ^2 appears in both the numerator and the denominator. However, the corresponding approximations for the average over the distribution of τ and m in Eq. (5) introduce negligible error in the determination of $\langle\tau\rangle$ only when the relevant τ and m values are in a narrow range.[9] This is not the case in the present experment because of the nonparabolicity and of the anisotropy of the energy surfaces.[22] Fortunately, the effect of the approximations in Eq. (5) on the accuracy of m_s is negligible, since m_s is determined, almost exclusively, from Eq. (4). However, the

optical mobilities are expected to be different from those measured from conductivity experiment because the mixing of τ and m occurs as reciprocal products at optical frequency, as can be seen for large $\omega\tau$ values,

$$2\eta\kappa = (Ne^2/\epsilon_0\omega^3)\langle 1/m\tau\rangle ,$$

while it occurs as quotients $\langle \tau/m\rangle$ in the steady-state conductivity.

B. Relationship of Susceptibility Mass to Energy Bands

Dixon and Riedl[2] developed equations from which m_s can be calculated for the Cohen model. These equations were derived from the Boltzmann equations assuming $\omega\tau \gg 1$. We would like to point out that this assumption is not always necessary, even when τ depends on energy, and that the validity of these equations can be extended to smaller $\omega\tau$ values. Equation (25) of Dixon and Riedl,[2] written without any assumption concerning $\omega\tau$ values, becomes

$$\epsilon_0\chi_c = \frac{1}{3}\frac{2e^2}{(2\pi)^3}\frac{\Gamma}{\hbar}\int_0^\infty \frac{\tau^2}{1+\omega^2\tau^2}\frac{\partial f_0}{\partial E} \times\left(\int_{s_k} v\, ds_k\right)_E dE , \quad (6)$$

where Γ is the number of equivalent valleys, $v = (1/\hbar)\nabla_k E$, and s_k is a constant-energy surface in k space. In many cases, such as the present experiment where $\omega\tau > 3$, the term $\tau^2/(1+\omega^2\tau^2)$ is, as explained before, a slowly varying function of energy E. For these cases, it can be averaged separately outside the integral using the same approximations as those involved in Eq. (4) with the introduction of negligible error (see Sec. III A). Using $\chi_c = \eta^2 - \kappa^2 - 1$, comparison of Eq. (6), approximated this way, with Eq. (4) (in which $\epsilon_t = 1$ for free-carrier dispersion only) gives also Eq. (26) of Dixon and Riedl[2]:

$$\frac{N_1}{m_s} = -\frac{1}{3}\frac{2}{(2\pi)^3}\frac{1}{\hbar}\int_0^\infty \frac{\partial f_0}{\partial E}\left(\int_{s_k} v\, ds_k\right)_E dE , \quad (7)$$

where $N_1 = N/\Gamma$ is the carrier concentration in one valley. Thus it is seen that Eq. (7) is valid for the same range of $\omega\tau$ values as was Eq. (4).

For all the models used in this paper (Kane, Cohen, and Dimmock models), the constant-energy surfaces have an axis of revolution, and we may write[2]

$$ds_k = 2\pi k_T\, dk_L\,[\nabla_k E/\,|(\nabla_k E)_T|\,] ,$$

in which the factor in square brackets projects the cylindrical dk_L element on the surface of constant energy, and k_T and k_L are the transverse and longitudinal wave numbers, respectively. The final equation, valid for $\omega\tau > 3$ in the present case, is[2]

$$\frac{N_1}{m_s} = \frac{-4}{3\hbar^2(2\pi)^2}\int_0^\infty \frac{\partial f_0}{\partial E} \times\left(\int_0^{k_{L\,\max}} \frac{|\nabla_k E|^2 k_T}{|(\nabla_k E)_T|}\, dk_L\right)_E dE , \quad (8)$$

in which

$$N_1 = \frac{N}{\Gamma} = \int_0^\infty -\frac{\partial f_0}{\partial E} H(E)\, dE ,$$

where

$$H(E) = \frac{2}{(2\pi)^2}\int_0^{k_{L\,\max}} k_T^2\, dk_L .$$

Equations (8) and (4) form the link between the measured susceptibility effective mass and the energy-band models. Given the energy dispersion $E(\vec{k})$, we can find $k_{L\,\max}$, k_T^2, and $[\,|\nabla_k E|^2/|(\nabla_k E)_T|\,]k_T$ and integrate Eq. (8) analytically or numerically to obtain the calculated mass m_s. In turn, it is the same quantity m_s (as shown above) which is obtained from the experiment using Eqs. (4) and (5).

IV. METHOD OF ANALYSIS

The various methods of analysis by which some or all of the parameters N or m_s, ϵ_∞, and μ_{opt} are determined from Eqs. (1), (4), and (5) have first been developed[2,9,21,23,24] under the assumption that $\epsilon_t = \epsilon_\infty$ and $a^2 = 1$. The contribution of $\Delta\epsilon_\infty(\lambda)$ is usually detected[24] as an abrupt increase in reflectivity with decreasing wavelengths starting at about the absorption edge. For all the present samples, the absorption edge, estimated as the main gap[25] plus a Burstein shift equal to the Fermi energy (see Fig. 13), was outside the range of wavelengths used in all cases. Also, the experimental reflectivity did not deviate from the calculated free-carrier dispersion curves (see Fig. 5) by more than 2% at the shortest wavelengths, corresponding to a value of $\Delta\epsilon_\infty/\epsilon_\infty$ less than 5%. Moreover, $\Delta\epsilon_\infty(\lambda)$ decreases rapidly with increasing wavelengths and may be neglected at the position of the reflectivity minimum. The relative contribution of the lattice dispersion was estimated using[16,26]

$$(1-\epsilon_\infty/\epsilon_s)(\lambda^2/\lambda_L^2) \simeq 0.9(\lambda^2/\lambda_L^2)$$

and the interpolated values of λ_L versus alloy composition.[27] It was found to be less than 6% at 22 μ in all cases, and less than 3% at the position of the reflectivity minimum in all but the three lowest carrier-concentration samples.

The assumption that $a^2 = 1$ has been found to in-

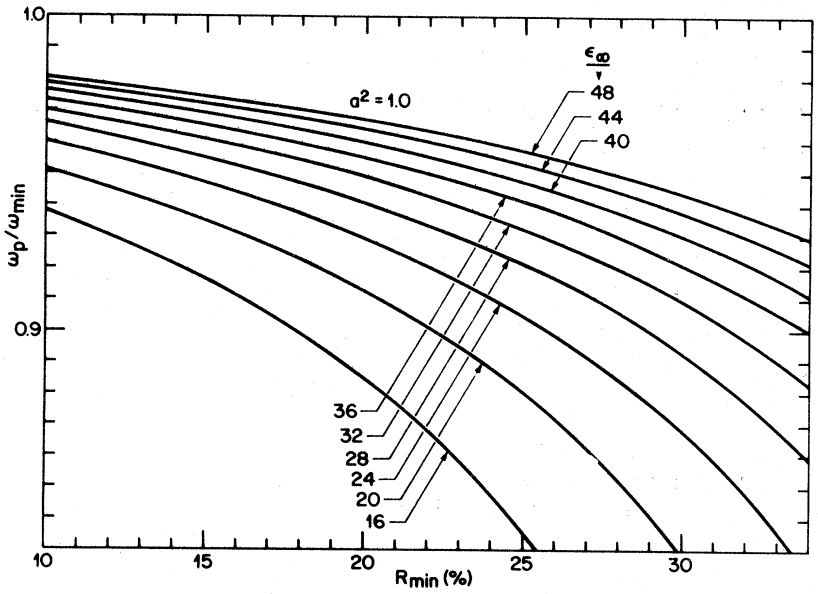

FIG. 1. Relation between plasma frequency and minimum reflectivity.

troduce negligible errors at low temperature in most cases of interest.[21] However, at higher temperatures when there is a distribution of scattering times and the condition $\omega^2\tau^2 \gg 1$ is not well satisfied, this assumption has been found to introduce appreciable errors in the determination of susceptibility effective masses.[19] The method of analysis first proposed by Lyden[21] has been extended[19] to these cases by using $a^2 \neq 1$ in Eq. (4). Here we extend the Moss *et al.* technique to cover these cases as well. The equations given below reduce to those of Moss *et al.*[9] when $a^2 = 1$.

We start from Eqs. (1), (4), and (5) with $\epsilon_t = \epsilon_\infty$ and find the conditions for a minimum in reflectivity. Differentiating

$$(1+R)/(1-R) = (\eta^2 + \kappa^2 + 1)/2\eta$$

with respect to κ^2 and equating to zero gives the condition[9]

$$\frac{d\eta}{d(\kappa^2)} = \frac{\eta}{1+\kappa^2-\eta^2} \quad . \tag{9}$$

Manipulation of Eqs. (4) and (5) to eliminate ω leads to

$$(\epsilon_\infty - \eta^2 + \kappa^2)\left(a^2 + \frac{(\epsilon_\infty - \eta^2 + \kappa^2)^2}{4\eta^2\kappa^2}\right) = \frac{a^4 N e^2 \langle\tau\rangle^2}{m_s \epsilon_0} \quad , \tag{10}$$

which after differentiation with respect to κ^2 gives

$$\frac{d\eta}{d(\kappa^2)} = \frac{\eta}{2\kappa^2} \times \frac{[2\kappa^2 + 3\epsilon_\infty + (4a^2-3)\eta^2]\kappa^4 - (\epsilon_\infty - \eta^2)^3}{[2\eta^2 - 3\epsilon_\infty + (4a^2-3)\kappa^2]\eta^4 + (\epsilon_\infty + \kappa^2)^3} \quad . \tag{11}$$

From Eqs. (9) and (11), we obtain the following relation between η and κ at the reflectivity minimum:

$$\kappa^2(5\eta^2 + 3\epsilon_\infty - 2) = (\epsilon_\infty - \eta^2)(\eta^2 - 1) - \frac{4\eta^2\kappa^4 a^2(3\eta^2 - \kappa^2 - 1)}{(\epsilon_\infty - \eta^2 + \kappa^2)^2} \quad , \tag{12}$$

in which the last term on the right-hand side is negligible for $\omega^2\tau^2 \gg 1$.

Writing $\omega_p^2 \equiv Ne^2/m_s\epsilon_0\epsilon_\infty$ (ω_p is the plasma frequency) in Eqs. (4) and (5), we obtain

$$\frac{\omega_p^2}{\omega^2} = \frac{\epsilon_\infty + \kappa^2 - \eta^2}{\epsilon_\infty} + \frac{4\eta^2\kappa^2 a^2}{\epsilon_\infty(\epsilon_\infty + \kappa^2 - \eta^2)} \quad , \tag{13}$$

$$\omega\langle\tau\rangle a^2 = \frac{\epsilon_\infty + \kappa^2 - \eta^2}{2\eta\kappa} \quad . \tag{14}$$

For given values of ϵ_∞ and a^2, pairs of η_{min}, κ_{min}, satisfying Eq. (12) at the minimum reflectivity, can be found and the corresponding R_{min}, ω_p/ω_{min}, and $\omega_{min}\langle\tau\rangle a^2$ values calculated using Eqs. (1), (13), and (14), respectively. From plots of ω_p/ω_{min} and $\omega_{min}\langle\tau\rangle a^2$ versus R_{min} for different values of ϵ_∞ and a^2, it is then possible to determine $\langle\tau\rangle$ and ω_p knowing the experimental values of R_{min} and ω_{min} only. ω_p/ω_{min} versus R_{min} is plotted in Figs. 1 and 2 for $a^2 = 1$ and $a^2 = 2$, respectively, while $\omega_{min}\langle\tau\rangle a^2$ versus R_{min} is plotted in Fig. 3. In all graphs, curves are shown for several values of ϵ_∞. For intermediate values of a^2 or ϵ_∞, a linear interpolation is sufficiently accurate.

In the present experiment, both the fitting techniques and the Moss *et al.* technique (modified as above) were used. Good fits are always required to ascertain the accuracy of the results obtained

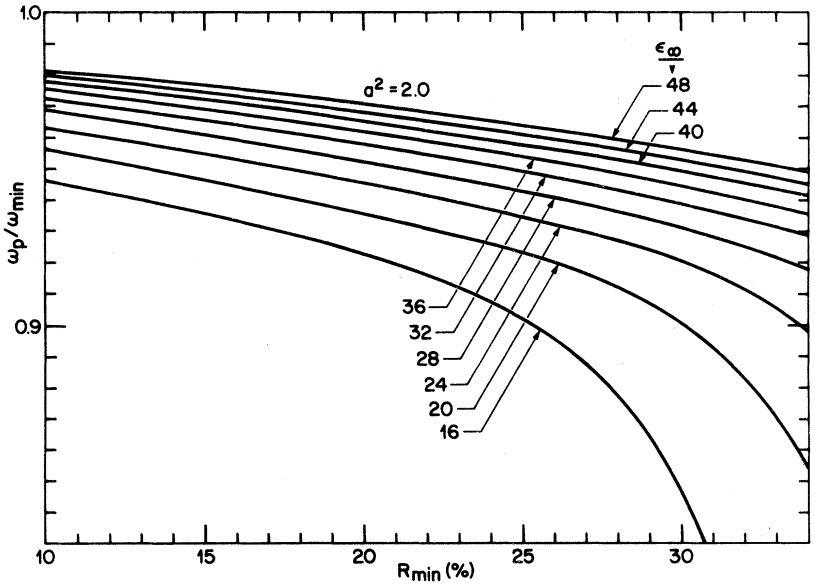

FIG. 2. Relation between plasma frequency and minimum reflectivity.

from any method of analysis. Also, the fitting technique has the advantage that none of the parameters ϵ_∞, m_s, and μ_{opt} need to be determined independently. With the Moss *et al.* technique, ϵ_∞ is found from an independent measurement, the accuracy of which limits that of the parameters m_s and μ_{opt} obtained from the analysis. However, the fitting technique is very sensitive to deviation from the absolute reflectivity. To illustrate this we have reanalyzed our experimental reflectivity spectra after they had been multiplied by 0.95 (a hypothetical correction factor for an aluminum mirror which is 95% reflecting). This 5% hypothetical error in absolute reflectivity was not detectable using the fitting technique because the quality of the fit was comparable with that obtained on the original spectra. But, the values of m_s, μ_{opt}, and ϵ_∞ so obtained were 16–11% higher, 23–15% lower, and 13–10% lower than the original ones, respectively, in going from high to low carrier concentrations. In contrast, using the Moss *et al.* technique, the corresponding values of m_s and μ_{opt} were 2.4–0.4% lower and 7–4% larger than the original ones. In addition, using the Moss *et al.* technique, the condition $\epsilon_t = \epsilon_\infty$ (i.e., negligible values of $\Delta\epsilon_\infty$ and ϵ_{LV}) needs to be satisfied for wavelengths near the reflectivity minimum only and, as discussed earlier, it is generally better satisfied there than in other parts of the spectrum. As will be seen in Sec. V, there were additional advantages to the use of both methods of analysis in the present experiment.

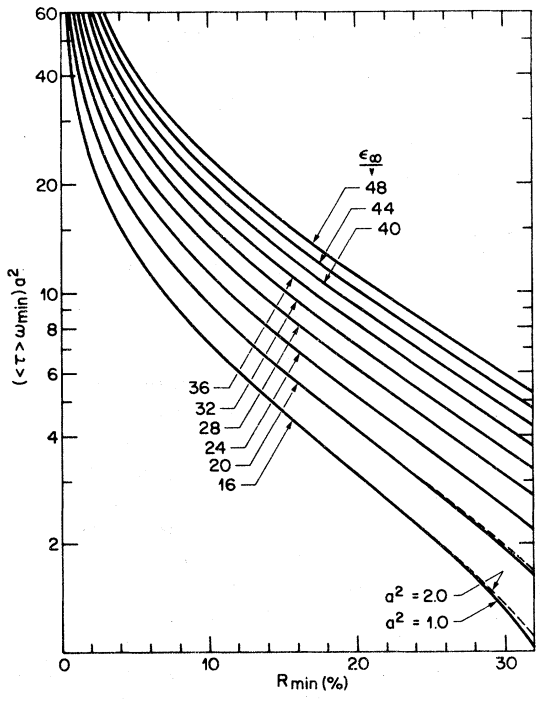

FIG. 3. Relation between scattering time and minimum reflectivity.

V. RESULTS AND DISCUSSION

A. Optical Dielectric Constant

The values of the optical dielectric constant ϵ_∞, measured in samples 8-8 and 6-3 at 82 and 300 °K, are listed in Table II together with those available for PbTe.[28,29] For these low carrier-concentration alloy samples, the reflectivity was constant for an appreciable range of wavelengths around 10 μ because the free-carrier dispersion ϵ_{FC}, $\Delta\epsilon_\infty(\lambda)$, and ϵ_{LV} were negligbile at these wavelengths.

TABLE II. Optical dielectric constant measured at 82 and 300 °K in $Pb_{1-x}Sn_xTe$.

Sample No.	x	ϵ_∞(82 °K)	ϵ_∞(300 °K)
8-8	0.208	43.3	40.5
6-3	0.06	38.8	34.5
PbTe [a]	0	36.8	31.8

[a]From Refs. 28 and 29.

Thus ϵ_∞ was found from the reflectivity at these wavelengths using $\epsilon_\infty = [(R^{1/2}+1)/(1-R^{1/2})]^2$. Each measurement of ϵ_∞ was repeated three times (each time on a repolished surface), thus giving an accuracy of about 5% for the estimated 3% error in the absolute reflectivity. It is seen from Table II that there is a relation between ϵ_∞ and E_G in PbTe and in the lead-rich $Pb_{1-x}Sn_xTe$ alloys investigated: ϵ_∞ increases when E_G decreases owing to decreasing temperature or increasing SnTe content. Figure 4, a semilogarithmic plot of E_G[25,30] versus the corresponding values of ϵ_∞ given in Table II, gives the following empirical relationship:

$$\ln E_G = -0.086\epsilon_\infty + 1.65 \ . \tag{15}$$

The empirical relationship[17] $\epsilon_\infty^2 E_G$ = "constant," which was found to be obeyed quite well in several semiconducting compounds,[17] is also plotted (dotted line) for comparison. The "constant" was chosen to fit the room-temperature data for PbTe. As seen, the latter relation does not fit our experimental results. The logarithmic form of the empirical relation (15) may be justified as follows.

The optical dielectric constant is given by[17]

$$\epsilon_\infty - 1 = \frac{2}{\pi}\int_0^\infty 2\eta\kappa \frac{dE}{E} \ , \tag{16}$$

in which $d\lambda/\lambda = -dE/E$ has been used. The $2\eta\kappa$ curve for p-type PbTe is given versus wavelength by Moss[17] and is reproduced schematically in the insert at the top of Fig. 4. On replotting as $2\eta\kappa/\lambda$ and integrating graphically over all wavelengths, Moss[17] found $\epsilon_\infty = 30.3$ in good agreement with the experimental value of 31.8 given in Table II. An important characteristic of this $2\eta\kappa$ curve is that the value of $2\eta\kappa$ is close to a constant on the short-wavelength side of the absorption edge for an appreciable range of wavelengths, i.e., a photon energy range from E_G to some value E_{pl}. Thus, the $2\eta\kappa$ curve may be approximated by a constant value $(2\eta\kappa)_{pl}$ in this range and by zero for energies below E_G. By choosing a convenient value of the energy E_{pl}, Eq. (16) may be integrated in two parts, from ∞ to E_{pl} and from E_{pl} to E_G. In view of the similarity of the band structure in PbTe and the lead-rich $Pb_{1-x}Sn_xTe$ alloys,[22,31] the above model for PbTe was carried over to the alloys and both E_{pl} and $(2\eta\kappa)_{pl}$ were assumed to be the same in the alloys as in PbTe. If, in addition, the contribution of the integral from ∞ to E_{pl} is taken to be the same for all samples measured, the integration gives

$$\ln E_G = -\frac{\epsilon_\infty}{(2/\pi)(2\eta\kappa)_{pl}} + A \ . \tag{17}$$

This is Eq. (15) with $A = 1.65$ and $(2\eta\kappa)_{pl} = 18.2$. The fact that Eq. (17) fits our experimental result and that it yields a value of $(2\eta\kappa)_{pl}$ close to that measured in PbTe (i.e., 16.5) suggests that the assumptions of the above model are reasonable.

B. Susceptibility Effective Mass

Figure 5 shows some of the experimental reflectivity data obtained at 82 °K together with the calculated best fit. The fitting parameters $M_s = m_s/m_0$, ϵ_∞, and μ_{opt} corresponding to the best fit are shown on each graph. In all cases, the experimental reflectivities are remarkably well fitted by the classical free-carrier dispersion model. In order to extract more information from the experimental data, the reflectivity measurements were analyzed using the Moss *et al.* technique also. Table III lists the data obtained from the reflectivity minimum.

The susceptibility effective masses obtained from both methods of analysis are compared in

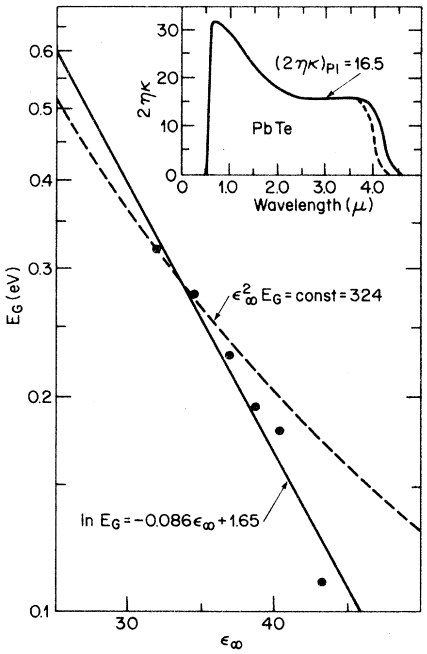

FIG. 4. Relation between energy gap and optical dielectric constant. The values of E_G are from Refs. 25 and 30. The values of ϵ_∞ are from Table II. The insert shows the $2\eta\kappa$ spectra for PbTe, taken from Ref. 17, from which ϵ_∞ can be calculated.

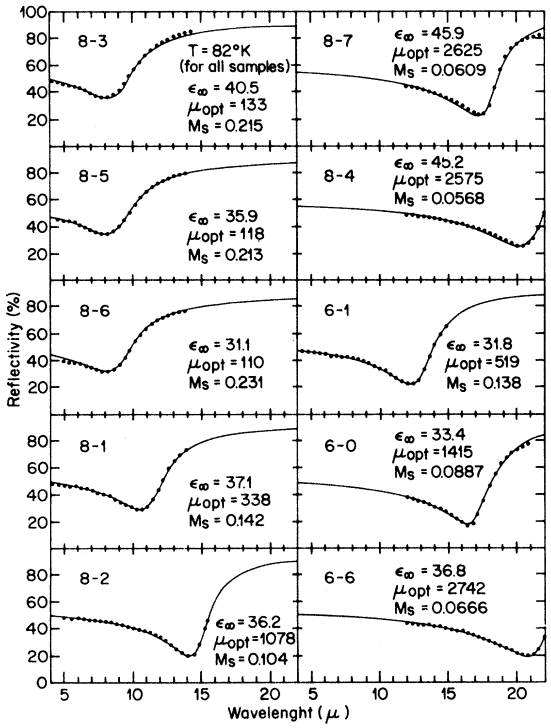

FIG. 5. Experimental (points) and calculated (solid curves) reflectivity spectra. The calculation was based on classical free-carrier dispersion relations, as discussed in the text. The dispersion parameters, corresponding to the best fit shown, are given on each graph. The temperature of the measurements is 82 °K in all cases.

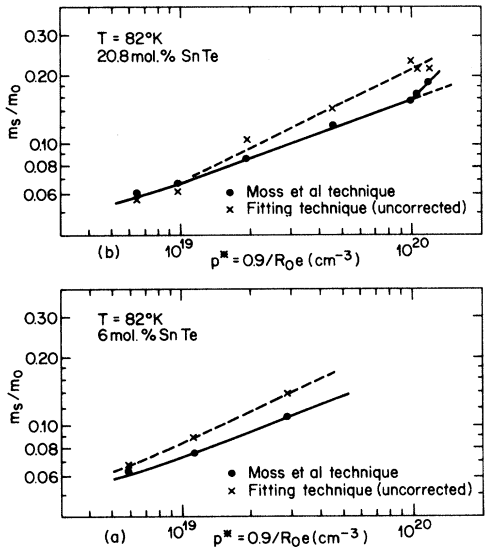

FIG. 6. Variation of the susceptibility hole mass m_s/m_0 with p^* at 82 °K in $Pb_{1-x}Sn_xTe$ alloys with (a) 6-mol% SnTe and (b) 20.8-mol% SnTe. There is an apparent disagreement between the experimental values of m_s/m_0 obtained from the two methods of analysis used as explained in the text.

Fig. 6. These results were obtained using the values of the Hall factor r and of the optical dielectric constant ϵ_∞ measured independently on low carrier-concentration samples and given earlier. The discrepancy between the two curves arises because the curve-fitting technique neglects the variation of r with carrier concentration while the Moss *et al.* techniques neglect mainly the variation of the ratio r/ϵ_∞ with carrier concentration. The kink observed in the full curve indicates an abrupt change in either ϵ_∞, r, or m_s (or several of them) and is taken as evidence for the presence of a second valence-band maximum. This second valence-band maximum was detected[32] also in the electrical results which indicated in addition that it is a heavy-mass band maximum compared to the main ⟨111⟩ maxima.

Figure 7(b) shows a semiempirical curve of the Hall factor r versus carrier concentration. We

TABLE III. Data obtained from the reflectivity minimum at 82 °K in $Pb_{1-x}Sn_xTe$ samples with different hole concentrations.

Sample No.	η_{min}	κ_{min}	λ_{min} (μ)	R_{min} (%)	ω_p/ω_{min}	$\omega_{min}\langle\tau\rangle$	M_s	μ_{opt} (cm^2/V sec)
				20.6-mol% SnTe (T = 82 °K)				
8-3	3.37	1.33	7.96	35.30	0.913	3.75	0.1890	134
8-5	3.23	1.30	8.02	33.95	0.920	4.10	0.1674	148
8-6	2.91	1.23	8.06	30.72	0.933	5.04	0.1537	172
8-1	2.75	1.19	10.52	28.95	0.940	5.65	0.1200	426
8-2	2.07	0.92	14.12	19.40	0.964	10.27	0.0862	1452
8-7	2.18	0.98	17.37	21.29	0.960	9.17	0.0667	2140
8-4	2.44	1.08	20.39	24.90	0.952	7.30	0.0614	2203
				6-mol% SnTe (T = 82 °K)				
6-1	2.22	0.97	12.28	21.50	0.955	8.12	0.1096	680
6-0	1.92	0.84	16.50	16.82	0.965	11.20	0.0751	1970
6-6	2.05	0.90	20.92	18.95	0.961	9.61	0.0633	2715

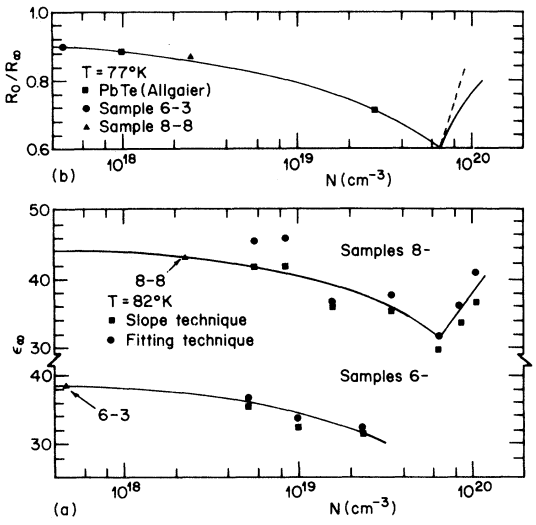

FIG. 7. Variation of (a) the optical dielectric constant ϵ_∞, and (b) the Hall factor R_0/R_∞ with carrier concentration N in $Pb_{1-x}Sn_xTe$ alloys at low temperature.

have assumed for carrier concentrations below the kink, that r varies in the same way in PbTe and $Pb_{1-x}Sn_xTe$ alloys with $x = 0.06$ and 0.21, on the basis that their ratio of longitudinal to transverse band-edge mass $K = m_L/m_T$ is the same[22] and that their band structure is similar.[22,31] Thus, the experimental values of r measured in the low carrier-concentration samples 6-3 and 8-8 (with $x = 0.06$ and 0.21, respectively) were plotted together with those measured by Allgaier[7,33] in PbTe. For carrier concentrations just past the kink, we have assumed that r behaves as is expected theoretically and indicated by the dotted line $r = 0.6N/N_1$ (where 0.6 is the extrapolated value of r at the kink and N_1 is the carrier concentration in the main $\langle 111 \rangle$ extrema at the kink). This simple relation is obtained because immediately past the kink, most extra carriers go into the heavy-mass band because of its high density of states and do not contribute appreciably to conduction. As the number of heavy-mass carriers is increased further, r deviates from the simple relation as indicated by the solid curve in Fig. 7(b). The experimental values of ϵ_∞ versus carrier concentration are those obtained from the reflectivity spectra using the curve-fitting and the slope techniques. These results are very similar to those obtained[34] in SnTe, in that ϵ_∞ decreases with increasing carrier concentration and then shows a kink when the second valence band becomes populated. Past this kink, while ϵ_∞ is constant in SnTe, it appears to increase in the alloys studied. This increase could not be explained. The gradual decrease in ϵ_∞ versus carrier concentration before the kink may be explained in terms of the Burstein shift of the fundamental absorption edge as was the case for SnTe.[24] Replacement of E_G by $E_G + E_F$ in Eq. (15) gives approximately the observed values of ϵ_∞ versus carrier concentration. It is to be noted that the ratio r/ϵ_∞ is close to a constant for various carrier concentrations. Finally, we would like to point out that the curve of r versus carrier concentration calculated by Tsu, Howard, and Esaki[35] for SnTe is very similar (except for the position of the kink) to that shown in Fig. 7(b) for the alloys studied. This appears to be a further justification for the assumptions used above concerning r in $Pb_{1-x}Sn_xTe$ alloys. While experimental measurements do not confirm the presence of a kink in SnTe,[36] they are consistent with its presence according to Tsu, Howard, and Esaki.[35] This point has also been discussed by Bis and Dixon.[14]

Figure 8 gives the susceptibility effective masses now corrected for the above variation of r and ϵ_∞ with carrier concentration. The values of m_s determined from the Moss *et al.* technique are the same after correction as those of Fig. 6 (to better than 5%) and are reproduced unchanged. This is mainly because r/ϵ_∞ is close to a constant at all carrier concentrations. But those determined from the fitting technique are now lower, after correction, and agree well with those determined from the Moss *et al.* technique. The discrepancy still remaining for two points was attributed to experimental errors in the reflectivity measurements, such as deviation from the absolute reflectivity to which the fitting technique is particularly sensitive. In fact, these two samples gave the worst fits.

Figure 9 shows the final result, this time with $N = r/R_0e$ as abscissa. The kink is now almost absent suggesting that the effective mass in the heavy-hole band is not too different from that in the light-hole band at the carrier concentration of the kink. Also it is seen that this kink would have gone undetected if only the fitting technique

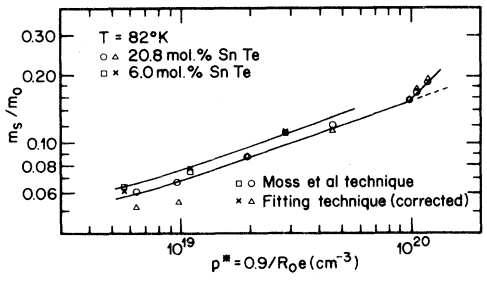

FIG. 8. Variation of the susceptibility hole mass m_s/m_0 with p^* at 82 °K in $Pb_{1-x}Sn_xTe$ alloys with 6-mol% SnTe and 20.8-mol% SnTe. The values of m_s/m_0 are corrected for the variation of r and ϵ_∞ with carrier concentration as explained in the text.

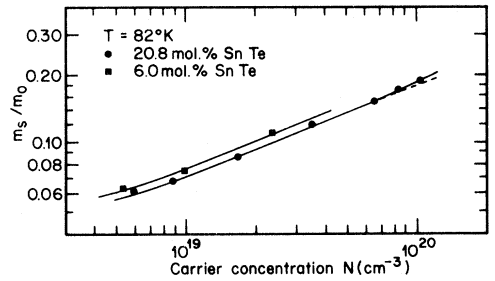

FIG. 9. Variation of the susceptibility hole mass m_s/m_0 with carrier concentration N at 82 °K in $Pb_{1-x}Sn_xTe$ alloys, with 6-mol% SnTe and 20.8-mol% SnTe. Only the values of m_s/m_0 determined from the minimum reflectivity technique are shown.

had been used. Only the results obtained from the Moss *et al.* technique are shown in Fig. 9 because, as seen earlier, they are more accurate in the present case.

Table IV lists the values of m_s and μ_{opt} obtained in sample 8-7 between 82 and 300 °K. The values of ϵ_∞ were obtained by linear interpolation between the experimentally determined values at room temperature and 82 °K. The values of m_s and μ_{opt} corrected for carrier scattering ($a^2 \neq 1$) are given in the last columns. The values of a^2 necessary to find these corrections were estimated using the Kane model, described below, with a value of E_G found from linear interpolation between the measured values at 82 and 300 °K.[25,30] For these calculations, isotropic acoustic scattering was assumed at all temperatures. A contribution from impurity scattering is also expected[37] at lower temperatures, but for sample 8-7 the calculated values of a^2 were about the same from 82 to 200 °K for both types of scattering. As seen from Table IV, accurate values of a^2 are not required to correct m_s, since in the worse case (room temperature) a 40% increase in a^2 leads to only a 4% decrease in m_s. The correction soon becomes negligible as the temperature is lowered because $\omega_{min}\langle\tau\rangle$ values increase while a^2 decreases. The correction for μ_{opt} is, however, large: It is 36 and 4% at room temperature and 82 °K, respectively.

C. Optical Mobility

The optical mobility determined from the experimental reflectivity, using the Moss *et al.* technique is given in Figs. 10 and 11 together with the conductivity mobility. The conductivity mobility was calculated from $\mu_c = \sigma(T)/Ne$, in which $\sigma(T)$ is the conductivity at temperature T. Both μ_c and μ_{opt} show similar variation with carrier concentration and temperature but μ_{opt} is always lower than μ_c by a factor of approximately 2. This has also been observed in PbTe[2] and in SnTe.[14,24] As the thermal velocities of the carriers are hardly affected by the small electric field in either optical or conductivity experiments, $\langle\tau\rangle$ should depend only

TABLE IV. Data obtained from the reflectivity minimum at several temperatures in a $Pb_{0.792}Sn_{0.208}Te$ sample with 8.68×10^{18} holes cm^{-3}.

						Uncorrected		Corrected		
T (°K)	ϵ_∞	R_{min} (%)	λ_{min} (μ)	ω_p/ω_{min}	$\omega_{min}\langle\tau\rangle$	M_s	μ_{opt} (cm^2/V sec)	M_s	μ_{opt} (cm^2/V sec)	a^2
84.0	43.3	22.10	17.30	0.9587	8.79	0.0658	2157	0.0658	2074	1.04
87.5	43.3	22.53	17.36	0.9578	8.55	0.0664	2087	0.0664	1997	1.04
93.6	43.2	22.80	17.40	0.9570	8.37	0.0670	2030	0.0670	1933	1.05
101.0	43.0	22.98	17.46	0.9564	8.22	0.0678	1975	0.0678	1863	1.06
110.3	42.9	23.48	17.54	0.9551	7.97	0.0688	1897	0.0688	1773	1.07
122.4	42.8	24.30	17.69	0.9530	7.52	0.0705	1762	0.0705	1624	1.08
132.2	42.7	24.72	17.80	0.9517	7.32	0.0717	1696	0.0717	1542	1.10
143.2	42.5	25.65	17.97	0.9491	6.85	0.0738	1557	0.0738	1403	1.11
155.3	42.4	26.45	18.11	0.9467	6.51	0.0755	1457	0.0755	1289	1.13
165.8	42.2	27.30	18.29	0.9440	6.14	0.0779	1347	0.0779	1176	1.14
178.4	42.0	28.48	18.44	0.9398	5.65	0.0802	1213	0.0802	1041	1.16
188.6	41.9	29.30	18.54	0.9367	5.33	0.0818	1128	0.0818	952	1.18
198.7	41.8	30.50	18.76	0.9320	4.92	0.0848	1016	0.0848	847	1.20
212.2	41.6	31.20	19.00	0.9290	4.68	0.0880	943	0.0880	770	1.22
221.5	41.5	31.97	19.24	0.9255	4.43	0.0911	873	0.0910	704	1.24
228.9	41.4	32.80	19.34	0.9215	4.20	0.0931	814	0.0923	651	1.25
240.3	41.3	33.46	19.64	0.9181	4.02	0.0970	760	0.0960	598	1.27
251.4	41.1	34.40	20.00	0.9129	3.76	0.1022	687	0.1005	533	1.29
261.6	41.0	35.30	20.18	0.9076	3.55	0.1055	633	0.1035	485	1.30
272.6	40.9	36.56	20.46	0.8992	3.24	0.1108	558	0.1080	423	1.32
286.0	40.7	37.54	20.65	0.8915	3.01	0.1154	503	0.1100	375	1.34
299.7	40.5	39.20	20.87	0.8785	2.67	0.1217	427	0.1170	314	1.36

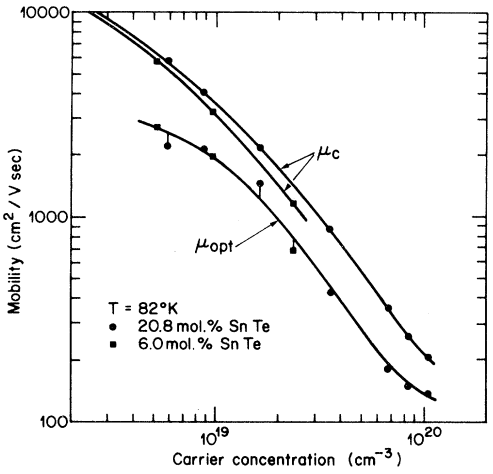

FIG. 10. Variation of conductivity and optical mobilities with carrier concentration at 82 °K in $Pb_{1-x}Sn_xTe$ alloys with 6-mol% SnTe and 20.8-mol% SnTe.

on the crystal properties and temperature[21] and should be the same in both types of experiment. However, as pointed out earlier, for a nonparabolic band τ and m are not separable in general and the nature of the average over the distribution is different in the two types of measurement. In the present case, at 82 °K the $\omega\tau$ values are large and the statistics are degenerate. Using $K = m_L/m_T$ and $b = \tau_L/\tau_T$ for the anisotropic energy surfaces, the quantity to be averaged in Eq. (5) is

$$\left\langle \frac{1}{m\tau} \right\rangle = \frac{(2Kb+1)(b+2)}{3b(2K+1)} \left\langle \frac{1}{m} \right\rangle \frac{1}{\langle \tau \rangle} .$$

On the other hand, we have

$$\mu_c = e \left\langle \frac{\tau}{m} \right\rangle = e \frac{3(2K+b)}{(2K+1)(b+2)} \left\langle \frac{1}{m} \right\rangle \langle \tau \rangle .$$

With these relations, Eq. (5) becomes

$$2\eta\kappa = \frac{Ne^3}{\epsilon_0 \omega^3} \frac{(2Kb+1)(2K+b)}{b(2K+1)^2} \left\langle \frac{1}{m} \right\rangle^2 \frac{1}{\mu_c} .$$

Thus, the quantity determined from the reflectivity measurements was

$$\frac{b(2K+1)^2}{(2Kb+1)(2K+b)} \mu_c .$$

For $K \simeq 13$ [22] and $b \simeq 3$ [33] this is about $0.95\mu_c$. This difference is small and does not account for the observed difference between the two types of mobility in Fig. 10.

The optical mobilities are not necessarily representative of the bulk since the light probes a very thin layer of material near the surface. If, for example, the mean free path of the electrons becomes comparable with the penetration depth, collisions with the surfaces reduce the scattering time or mobility. In the present case, the penetration depths at the reflectivity minimum, calculated using the κ values from Table III, ranged from 0.4 to 1.8 μ. A rough estimate of the mean free path $\Lambda \simeq v_F \langle \tau \rangle$, using $v_F = (2E_F/m_s)^{1/2}$, in which the pertinent values were taken from Fig. 13 and Table III, gave Λ ranging from 0.02 to 0.12 μ. The mean free path of the carriers is at most 8% of the penetration depth, and boundary scattering, while not negligible, cannot account quantitatively for the observed difference between the optical mobility and the conductivity mobility. It thus appears that most of the discrepancy between the two types of mobility has not yet been explained adequately and that perhaps it is due to different properties of the thin surface layers as compared to those of the bulk. For example, surface strains (improbable in the present case as indicated in Sec. II) or chemisorbed impurities are all expected to lower the mobility of the thin surface layer probed by the light.

VI. COMPARISON OF EXPERIMENT WITH VARIOUS BAND MODELS

A. Carrier-Concentration Dependence

1. Kane Model

We refer here to the simplified Kane model for which the dispersion relation is

$$\frac{\hbar^2 k_T^2}{2m_T} + \frac{\hbar^2 k_L^2}{2m_L} = E\left(1 + \frac{E}{E_G}\right) , \qquad (18)$$

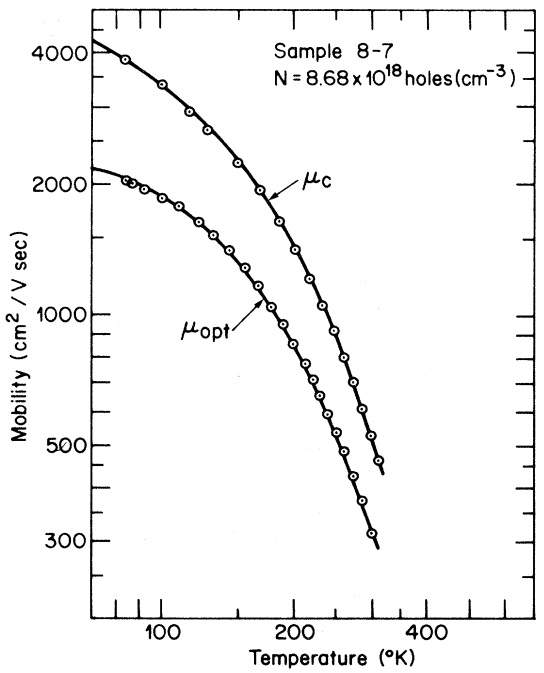

FIG. 11. Variation of conductivity and optical mobilities with temperature in $Pb_{0.792}Sn_{0.208}Te$ alloys with 8.68×10^{18} holes cm^{-3}.

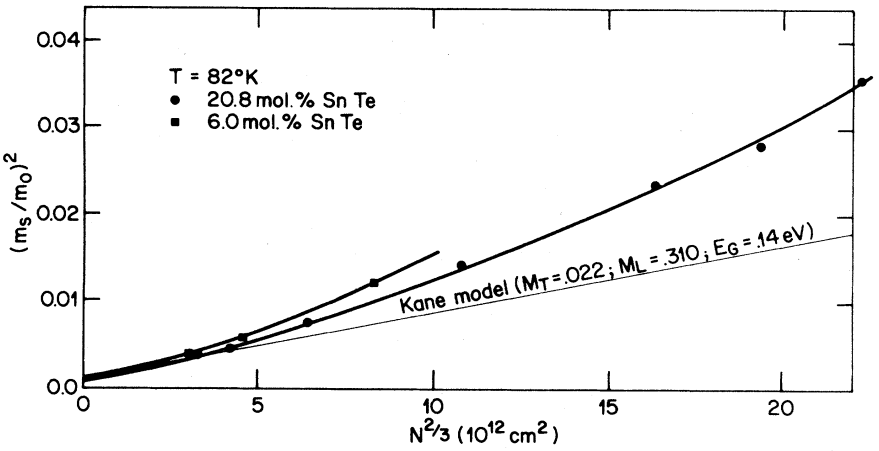

FIG. 12. Variation of $(m_s/m_0)^2$ with $N^{2/3}$. The Kane model is used for the calculated straight line.

in which k_T and k_L are the transverse and longitudinal wave numbers, m_T and m_L are the transverse and longitudinal band-edge masses, and E_G is the interaction gap. This model has been used[4] to explain the energy dependence of the density of states determined in p-type PbTe from the thermoelectric power in strong magnetic field. For carrier concentrations from 5.4×10^{17} to about 2×10^{19} cm^{-3}, these results[4] were well described by the Kane model with the parameters $E_G = 0.15$ eV and a density-of-states band-edge mass $m_d = 0.13m_0$.

The expression for the susceptibility effective mass for our degenerate samples at 82 °K is easily found from Eqs. (18) and (8), which can be integrated analytically to give

$$M_s^2 = M_c^2 + (4M_c^2/E_G M_d)(N/C)^{2/3}, \tag{19}$$

in which the M's are the susceptibility, band-edge conductivity, and band-edge density-of-states masses in electron-mass units, N is the carrier concentration in cm^{-3}, and $C = 18.17\times10^{21}$ cm^{-3}.

Thus, the susceptibility mass squared versus $N^{2/3}$ should be a straight line. Such a plot is shown in Fig. 12. As seen, the experimental results deviate more and more from the expected straight lines as the carrier concentration increases. For comparison, a theoretical curve has been plotted using $M_T = 0.022$, $M_L = 0.310$, and $E_G = 0.14$ eV. These band-edge parameters were determined for PbTe at 4.2 °K by Cuff *et al.*[1] Since the energy gap for $Pb_{1-x}Sn_xTe$ with $x = 0.06$ is about the same at 82 °K as it is for PbTe at 4.2 °K, the above parameters should apply to both cases. The theoretical and experimental curves for 6% SnTe alloys converge for carrier concentration less than about 10^{18} holes cm^{-3}. For both alloy compositions, we find that the Kane model does not explain our results for carrier concentrations in excess of 10^{18} cm^{-3}.

2. *Cohen Model*

The Cohen model has been used with some success in PbTe by Dixon and Riedl[2] to explain their experimental results of susceptibility effective mass versus carrier concentration. The dispersion relation describing the constant-energy surface is given in Dixon and Riedl[2] as

$$E = \frac{\hbar^2}{2}\left(\frac{k_T^2}{m_T}\,\frac{1}{1+(1/E_G)(E+\hbar^2k_L^2/2m_L')} + \frac{k_L^2}{m_L}\right), \tag{20}$$

in which m_L' is the longitudinal band-edge mass of the conduction electrons. The expression for m_s was obtained as before from Eqs. (20) and (8) as described in detail for the Cohen model by Dixon and Riedl.[2] For the alloys studied, the following band parameters were used: First, $m_L/m_L' = 1.3$, as determined[1] from Shubnikov–de Haas measurements in PbTe, was used for the alloys. The calculated values of m_s were very insensitive to this parameter. Second, $K = m_L/m_T$ was taken to be 13 as measured from Shubnikov-de Haas measurements by Burke *et al.*,[22] who found that K is independent of carrier concentration and alloy composition in $Pb_{1-x}Sn_xTe$ up to $x = 0.3$. Third, we assumed that the relation $m_T = E_G/(E_p - E_G)$ with $E_p = 6.4$ eV as determined by Cuff *et al.*[1] was valid in the alloys studied as well. As pointed out by Cuff *et al.*,[1] the interaction with the most remote energy levels at ⟨111⟩ is of secondary importance and the mass components are determined principally by the small gap between the valence and conduction bands. This suggests that the same relation may be used in the alloys studied, because of their small gap.

Figure 13 compares the experimental values of m_s with those calculated from the Cohen model. The values of $E_G = 0.16$ and 0.12 eV, in fair agreement with the optical gap, gave the best fits (the full curves) for the alloys with $x = 0.06$ and 0.21,

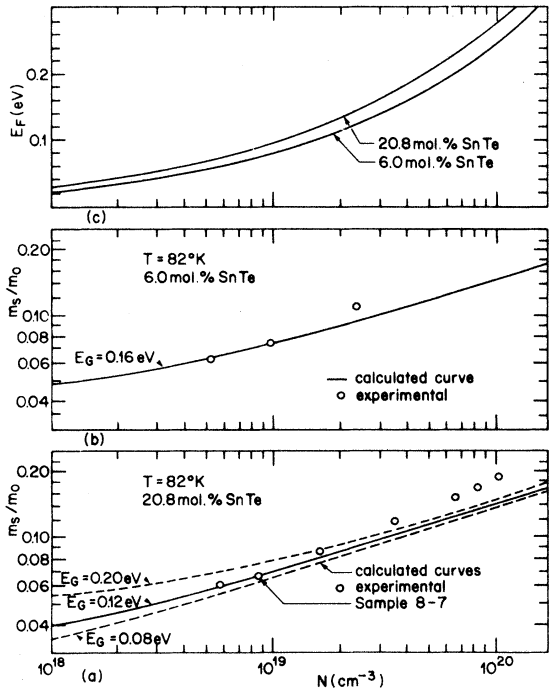

FIG. 13. Carrier-concentration dependence of the susceptibility hole mass m_s/m_0 at 82 °K in $Pb_{1-x}Sn_xTe$ alloys with (a) 20.8-mol% SnTe and (b) 6-mol% SnTe. (c) Corresponding carrier-concentration dependence of the Fermi energy. The Cohen model is used to calculate all curves.

respectively. It is seen that our experimental results versus carrier concentration at 82 °K are well explained by the Cohen model for carrier concentration up to about 2×10^{19} holes cm^{-3}. At higher carrier concentrations, in the alloy with $x=0.21$, part of the discrepancy may be attributed to the heavy-mass band. From the kink at 6.6×10^{19} holes cm^{-3} (Fig. 8) and the Cohen Fermi energy [Fig. 13(c)], this heavy-mass band is situated at 0.23 eV below the light-mass band in $Pb_{0.79}Sn_{0.21}Te$ at 82 °K.

3. *Dimmock Model*

Dimmock[31] has derived a dispersion relation for $Pb_{1-x}Sn_xTe$. He has treated the interaction between the valence and conduction band at ⟨111⟩ exactly, and included the interaction of the far removed bands at ⟨111⟩ as a second-order perturbation. Thus, the Dimmock model appears to be better founded in that it takes into account the interaction of six bands. All the parameters of the model were determined by Dimmock[31] using the results of Cuff *et al.*,[1] the positioning of the far removed bands, and the matrix elements of Lin and Kleinman.[5] The only explicit parameter left was E_G. The model equation is[31]

$$(\tfrac{1}{2}E_G+1.81k_L^2+3.38k_T^2-E)(-\tfrac{1}{2}E_G-0.87k_L^2-7.23k_T^2-E)=0.033k_L^2+0.536k_T^2\,, \quad (21)$$

in which E and E_G are in rydbergs (2 Ry ≡ 1 a.u.) and k is in atomic units. The zero of energy is taken at the center of the energy gap; E is positive for PbTe and negative for SnTe (going through zero at about $Pb_{0.6}Sn_{0.4}Te$); and E is positive for the conduction band and negative for the valence band. The susceptibility effective mass was calculated from Eq. (8) written in the same units as Eq. (21) (i.e., $\hbar^2$ equal to 1 and m_s in units of free-electron mass), using the expressions for the integrants given by Eqs. (A2)–(A4) in the Appendix. All integrations were performed numerically.

The calculated values of m_s are shown in Fig. 14(a) together with the experimental values. The three calculated curves shown are for E_G equal to 0.23, 0.19, and 0.11 eV. These values correspond to PbTe, $Pb_{0.94}Sn_{0.06}Te$, and $Pb_{0.79}Sn_{0.21}Te$, respectively. The corresponding Fermi energies are shown in Fig. 14(b). As can be seen, the Dimmock model does not account for our experimental results for any of the carrier concentrations measured. The failure of the Dimmock model in the present case appears to have its origin in the determination of the parameters of the model. For example, Overhof and Rossler's[6] band-calculation results disagree with those of Lin and Kleinman[5] (which were used by Dimmock) in that the far removed bands (all four of them) are situated farther away from the main gap. Dubrovskaya *et al.*[4] pointed out that, as the far removed bands are brought closer to the main gap, the nonparabolicity is reduced. Thus, if the results of Over-

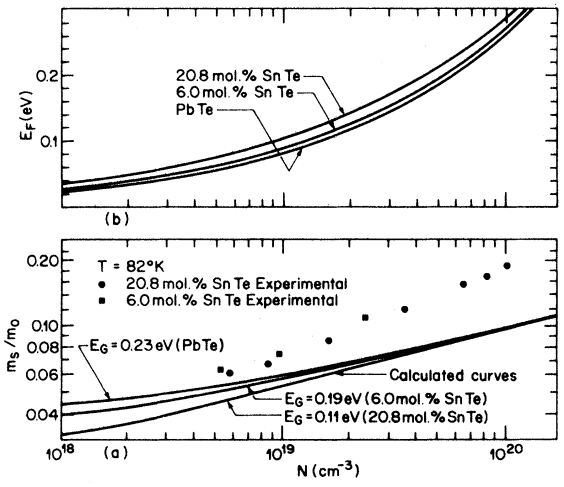

FIG. 14. (a) Carrier-concentration dependence of the susceptibility hole mass m_s/m_0 at 82 °K in $Pb_{1-x}Sn_xTe$ alloys with 20.8-mol% SnTe and 6-mol% SnTe. (b) Corresponding carrier-concentration dependence of the Fermi energy. The Dimmock model is used to calculate all curves.

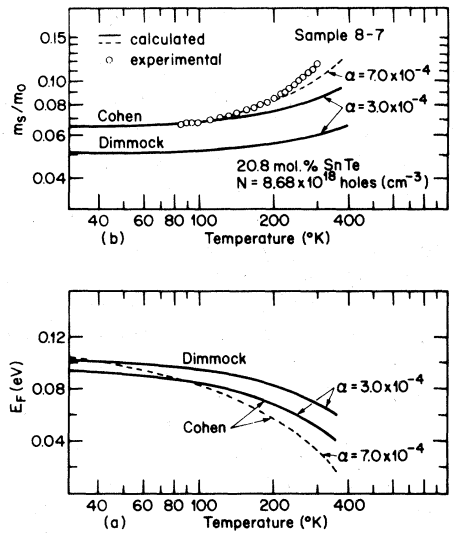

FIG. 15. Experimental (points) and calculated (full curves): (a) Fermi energy and (b) susceptibility hole mass vs temperature in $Pb_{0.792}Sn_{0.208}Te$ alloy with 8.68×10^{18} holes cm^{-3}. The Cohen and Dimmock models are used in the calculations as indicated.

hof and Rossler[6] are correct, the Dimmock model underestimates the nonparabolicity, as the experimental results indicate in Fig. 14.

B. Temperature Dependence

The experimental values of m_s in sample 8-7 from 82 to 300 °K (given in Table IV) are plotted in Fig. 15(b). They are compared with the values of m_s calculated using the two-band Cohen model and the six-band Dimmock model. The value of $E_G(T) = E_G(82\,°K) + \alpha(T - 82\,°K)$, in which $E_G(82\,°K) = 0.12$ eV and α is the linear variation coefficient of E_G with temperature (in eV/°K), was used in the calculation. For the experimentally determined[30] values of $\alpha \simeq 3 \times 10^{-4}$ eV/°K, none of the models accounts for the large increase observed in m_s with increasing temperature. The dotted line shows that the agreement is improved, with the Cohen model, for larger values of α. However, there are no justifications for using such large values of α. An alternative to using a large value of α would be to use in the relation between energy gap and the transverse mass found by Cuff *et al.*[1] at 4.2 °K, a value for the momentum parameter E_p which decreases with increasing temperature.

The discrepancy between the calculated and measured m_s near room temperature cannot be attributed to the heavy-mass band situated at about 0.23 eV below the light-mass band at 82 °K. Calculations for this sample indicate that this heavy-mass band is empty up to 250 °K at least, and that it contains less than 5% of the holes at 300 °K.

The Fermi energies corresponding to the calculated curves are given in Fig. 15(a).

VII. CONCLUSION

A. Experiment Accuracy of m_s

The results of m_s obtained using the Moss *et al.* method of analysis contain two types of error. The first type was statistical and was inherent in the method of analysis and the measurements. Repeated measurements involving remounting, repolishing (chemical), etc., indicated that the errors in the values of R_{min} and λ_{min} were less than 5 and 0.5%, respectively, thus contributing less than 2.5% error in m_s. The second type of error was a systematic one in the values of r and ϵ_∞ used. These systematic errors can be eliminated at a later date (starting with the m_s-vs-p^* results in Fig. 6) if more precise values of these parameters become available.

B. Valence-Band Structure

The kink observed in Fig. 6 at a hole concentration $N \simeq 6.6 \times 10^{19}$ cm^{-3} cannot be attributed to errors of the first type, and therefore it indicates an abrupt change of ϵ_∞, r, or m_s. This abrupt change is taken as evidence for the presence of a second valence band because ϵ_∞, r, and m_s are expected to vary smoothly with carrier concentration for a single band. The Fermi energy corresponding to the kink at 82 °K is found from Fig. 13(c) (Cohen model) to be 0.23 eV. This value does not change appreciably when using the Kane or Dimmock models. It thus appears that in $Pb_{1-x}Sn_xTe$ alloys with $x = 0.21$, there is an extra valence-band maximum 0.23 eV below the main one. In the alloys with $x = 0.06$, no such kink is observed up to carrier concentration 2.3×10^{19} cm^{-3} suggesting that the carriers are all in the main band for carrier concentrations lower than this.

For carrier concentrations below that of the kink ($< 6.6 \times 10^{19}$ cm^{-3}) the large increase of m_s with increasing carrier concentration, at 82 °K, was attributed to the nonparabolicity of the main ⟨111⟩ band. We found that the two-band Cohen model gave the best fit to our data and that the six-band Dimmock model was inadequate. This is surprising because the Dimmock model is better founded in that it takes into account the interaction of six bands at ⟨111⟩. However, as indicated above, the main assumptions leading to the Dimmock dispersion relation for $Pb_{1-x}Sn_xTe$ are questionable, and there is evidence that the model underestimates the nonparabolicity of the main ⟨111⟩ valence band. Also as pointed out by Dubrovskaya,[4] the success of the two-band models can be explained because of the considerable compensation of the effects of

the two higher and the two lower bands. Finally, the results of m_s versus temperature could not be accounted for by any of the models used. But, the Cohen model could provide a good fit by assuming a larger variation of the main gap with temperature than that measured experimentally, or alternatively by using a momentum parameter E_p which decreases with increasing temperature. Since the influence of the far removed bands is contained in E_p, this suggests that a six-band model is needed. Complete explanation of the experimental data thus probably requires an adequate six-band model of the ⟨111⟩ extrema in $Pb_{1-x}Sn_xTe$ alloys.

APPENDIX

In order to calculate the susceptibility effective mass for the Dimmock model,[31] expressions for $k_{L\,\max}$, k_T^2, and $[|\nabla_k E|^2/|(\nabla_k E)_T|]k_T$ are needed. To avoid carrying numbers through the long algebraic manipulations necessary to arrive at these expressions, Eq. (21) is rewritten as

$$(G + ak_L^2 + bk_T^2 - E)(G + ck_L^2 + ek_T^2 + E) + pk_L^2 + qk_T^2 = 0 , \tag{A1}$$

with $G = \frac{1}{2}E_G$, etc.

The limit of integration $k_{L\,\max}$ is obtained by writing $k_T^2 = 0$ in Eq. (A1). After a few algebraic manipulations we have

$$k_{L\,\max} = \left(\frac{-A_1}{2ac} \pm \frac{1}{2ac} \times [A_1^2 - 4ac(G+E)(G-E)]^{1/2}\right)^{1/2} , \tag{A2}$$

with

$$A_1 = (c+a)G + (a-c)E + p .$$

For the alloy compositions studied, the valence-band extrema are at the L point. Thus $k_{L\,\max}$ is equal to zero when $E = -G$, and only the positive sign is to be retained in Eq. (A2). This is not true for $Pb_{1-x}Sn_xTe$ with $x > 0.9$, since then the extrema occur at $k_L \neq 0$.[31]

The expression for k_T^2 also is obtained from Eq. (A1) and is

$$k_T^2 = -\frac{1}{2be}A_2 + \frac{1}{2be}\{A_2^2 - 4be[(G + ak_L^2 - E) \times (G + ck_L^2 + E) + pk_L^2]\}^{1/2} , \tag{A3}$$

with

$$A_2 = (e+b)G - (e-b)E + (ae+bc)k_L^2 + q .$$

The expression for $[|\nabla_k E|^2/|(\nabla_k E)_T|]k_T$ is found by implicit partial differentiation of Eq. (A1). The final result is

$$\frac{|\nabla_k E|^2}{|(\nabla_k E)_T|}k_T = \frac{2k_L^2[A_3 + (bc+ae)k_T^2]^2 + 2k_T^2(A_2 + 2bek_T^2)^2}{|[A_4 + (e-b)k_T^2](A_2 + 2bek_T^2)|} , \tag{A4}$$

in which

$$A_3 = [(a+c)G + 2ack_L^2 + (a-c)E + p] ,$$

$$A_4 = [2E - (a-c)k_L^2]$$

and A_2 is given above.

---

*Work based on a thesis submitted to the University of Ottawa by G. D. in partial fulfillment of the requirements of the Ph. D. degree in Physics.

[1]K. F. Cuff, M. R. Ellett, C. D. Kuglin, and L. R. Williams, in *Proceedings of the Seventh International Conference on Physics of Semiconductors, Paris*, 1964 (Academic, New York, 1965), p. 667.

[2]J. R. Dixon and H. R. Riedl, Phys. Rev. 138, A873 (1965).

[3]I. A. Chernik, V. I. Kaidanov, M. I. Vinogradova, and N. V. Kolomoets, Fiz. i Tekhn. Poluprov. 2, 773 (1968) [Sov. Phys. Semicond. 2, 645 (1968)].

[4]I. N. Dubrovskaya, Yu. I. Ravich, and O. S. Gryaznov, Fiz. i Tekhn. Poluprov. 3, 1770 (1969) [Sov. Phys. Semicond. 3, 1500 (1970)].

[5]P. J. Lin and L. Kleinman, Phys. Rev. 142, 478 (1966).

[6]H. Overhof and U. Rössler, Phys. Status Solidi 37, 691 (1970).

[7]R. S. Allgaier and B. B. Houston, Jr., J. Appl. Phys. 37, 302 (1966).

[8]H. J. Albany and M. Ocio, J. Phys. (Paris) Suppl. 29, C-4 125 (1968).

[9]T. S. Moss, T. D. F. Hawkins, and G. J. Burrell, J. Phys. C 1, 1435 (1968).

[10]E. Fortin, Rev. Sci. Instr. 41, 1252 (1970).

[11]G. Dionne and J. C. Woolley, J. Electrochem. Soc. 119, 784 (1972).

[12]D. G. Coates, W. D. Lawson, and A. C. Prior, J. Electrochem. Soc. 108, 1038 (1961).

[13]R. L. Weiker, Phys. Rev. 152, 736 (1966).

[14]R. F. Bis and J. R. Dixon, Phys. Rev. B 2, 1004 (1970).

[15]C. G. Darwin, Proc. Roy. Soc. (London) 152, A182 (1943).

[16]F. Stern, in *Solid State Physics*, edited by F. Seitz and D. Turnbull (Academic, New York, 1963), Vol. 15, pp. 229–408.

[17]T. Moss, *Optical Properties of Semiconductors; A Semiconductor Monograph* (Butterworths, London, 1959), pp. 17, 24, 29, 48, 189, and 192.

[18]P. A. Shumann and R. P. Phillips, Solid State Electron. 10, 943 (1967).

[19]B. Rheinländer, Phys. Letters (Netherlands) 29A, 420 (1969).

[20]B. Rheinländer, Phys. Status Solidi 38, 193 (1970).

[21]H. A. Lyden, Phys. Rev. 134, A1106 (1964).

[22]J. R. Burke, J. D. Jensen, and B. Houston, J. Phys. Chem. Solids Suppl. 32, 393 (1971).

[23]W. G. Spitzer and H. Y. Fan, Phys. Rev. 106, 882 (1957).

[24]H. R. Riedl, J. R. Dixon, and R. B. Schoolar, Phys. Rev. 162, 692 (1967).

[25]P. M. Nikolic, Brit. J. Appl. Phys. 18, 897 (1967).

[26]R. Dalven, Infrared Phys. 9, 141 (1969).
[27]K. W. Nill, J. N. Walpole, A. R. Calawa, and T. C. Harman, in *Proceedings of the Conference on Physics of Semimetals and Narrow Gap Semiconductors, Dallas*, 1970, edited by D. L. Carter and R. T. Bate (Pergamon, Oxford, 1971).
[28]J. N. Zemel, J. D. Jensen, and R. B. Schoolar, Phys. Rev. 140, A330 (1965).
[29]A. K. Walton and T. S. Moss, Proc. Phys. Soc. (London) B81, 509 (1963).
[30]R. N. Tauber and I. B. Cadoff, J. Appl. Phys. 38, 3714 (1967).
[31]J. O. Dimmock, in Ref. 27.
[32]G. Dionne and J. C. Woolley (unpublished).
[33]R. S. Allgaier, Phys. Rev. 119, 554 (1960).
[34]Y. Ota and S. Rabii, in Ref. 27.
[35]R. Tsu, W. E. Howard, and L. Esaki, Phys. Rev. 172, 779 (1968).
[36]B. B. Houston, R. S. Allgaier, J. Babiskin, and P. G. Siebenmann, Bull. Am. Phys. Soc. 9, 80 (1964).
[37]Yu. I. Ravich, J. Phys. (Paris) Suppl. 29, C-4 114 (1968).

PHYSICAL REVIEW B VOLUME 6, NUMBER 10 15 NOVEMBER 1972

Excitons Bound to Ionized Donors: Application of the Interparticle-Coordinates Method

S. G. Elkomoss
Laboratoire de Spectroscopie et d'Optique du Corps Solide, Institut de Physique, Strasbourg, France*
(Received 17 March 1972)

The interparticle-coordinates method given by Pluvinage and Walsh for helium and lithium atoms has been developed to apply to excitons bound to ionized donors. Good agreement with experiment for CdSe has been obtained. In these calculations the effect of the polarizability has been taken into account. This method can easily be generalized to apply to other exciton complexes of more than three particles.

I. INTRODUCTION

In a preceding paper,[1] the Pekeris method[2,3] for helium atoms had been developed extensively to apply to three-particle systems. Using this method, the binding energies for excitons bound to ionized donors have been calculated for several real systems of semiconductors. Good agreement with experiment has been obtained. Owing to the limitations of the use of the perimetric coordinates,[4–7] the Pekeris method cannot be developed for systems having more than three particles. On the other hand, for other observed exciton complexes having more than three particles, various authors[8–11] have used the Born–Oppenheimer approximation in their calculations. This approximation is usually valid for small ratios $\sigma = m_e^*/m_h^*$, where m_e^* and m_h^* are, respectively, the effective masses of the electron and the hole. For this reason, it is of considerable interest to develop a method that can be applied to systems of any number of particles and that is valid for any value of σ. The Pluvinage method[12,13] for helium generalized recently by Walsh[14–16] for lithium could satisfy such conditions. In this article, this method has been developed to apply, as an example, to three-particle systems. Comparison with experiment has been carried out for excitons bound to ionized donors in CdSe. Excellent agreement with experiment has been obtained. Owing to the success of this method for such exciton-ionized donor systems, its application to the different observed exciton complexes having more than three particles, are in progress. In these calculations, the effect of the polarizability has been taken into consideration and Haken's exciton potential has been adopted.[1,17]

II. METHOD OF SOLUTION

Let r_{12}, r_{13}, and r_{23} be, respectively, the distances between the donor and the electron, the donor and the hole, and the two particles in the exciton (Fig. 1). As described by Haken,[18] the dielectric constant $K(r_{23})$ between the hole and the electron of a delocalized exciton is a function of the distance r_{23}, of their effective masses, of the optical (K_0) and the static (K_s) dielectric constants, and of the longitudinal vibrational frequency ω of the lattice. Since atomic units in terms of a certain effective dielectric constant K_{eff} are usually adopted, the generalized Haken potential[17] for any two particles i and j of effective masses m_i^* and m_j^* in a crystal can be written in the following form:

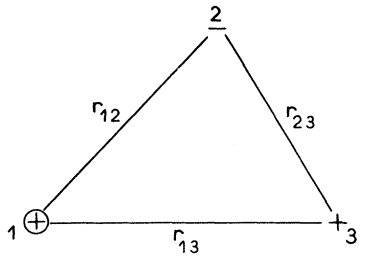

FIG. 1. Exciton-ionized donor complex.